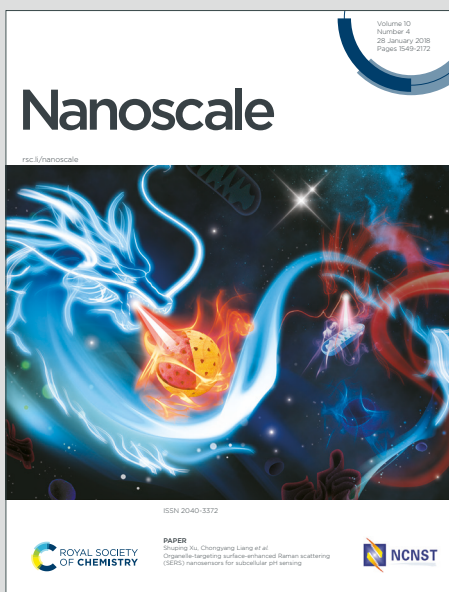


Nanoscale

Accepted Manuscript

This article can be cited before page numbers have been issued, to do this please use: S. MAJUMDER, G. Millette, T. Sackey, F. Malouin and S. George, *Nanoscale*, 2026, DOI: 10.1039/D5NR03837E.



This is an Accepted Manuscript, which has been through the Royal Society of Chemistry peer review process and has been accepted for publication.

Accepted Manuscripts are published online shortly after acceptance, before technical editing, formatting and proof reading. Using this free service, authors can make their results available to the community, in citable form, before we publish the edited article. We will replace this Accepted Manuscript with the edited and formatted Advance Article as soon as it is available.

You can find more information about Accepted Manuscripts in the [Information for Authors](#).

Please note that technical editing may introduce minor changes to the text and/or graphics, which may alter content. The journal's standard [Terms & Conditions](#) and the [Ethical guidelines](#) still apply. In no event shall the Royal Society of Chemistry be held responsible for any errors or omissions in this Accepted Manuscript or any consequences arising from the use of any information it contains.

1 **Chitosan conjugated cyclodextrin nanocomposite loaded with antibiotic-adjuvant**
2 **combinations remedies multi-drug resistant *Staphylococcus aureus* infection in CD-1 mice**
3 **model of bovine mastitis**

4 Satwik Majumder ^{a,b}, Guillaume Millette ^c, Trisha Sackey ^b, Francois Malouin ^c, Saji George ^{b*}

5 satwik.majumder@rutgers.edu

6 guillaume.millette@USherbrooke.ca

7 trisha.sackey@mail.mcgill.ca

8 francois.malouin@USherbrooke.ca

9 saji.george@mcgill.ca

10 ^a Environmental and Occupational Health Sciences Institute (EOHSI) and School of Public Health,
11 Rutgers University, Piscataway, NJ 08854, USA

12 ^b Department of Food Science and Agricultural Chemistry, Macdonald Campus, McGill
13 University, 21,111 Lakeshore Ste Anne de Bellevue, Quebec H9X 3V9, Canada

14 ^c Département de biologie, Faculté des sciences, Université de Sherbrooke, Sherbrooke, Quebec
15 J1K 2R1, Canada

16 *Corresponding author

17 Address of correspondence

18 Department of Food Science and Agricultural Chemistry, Macdonald-Stewart Building, Room-
19 1039, Macdonald Campus, McGill University 2111 Lakeshore, Ste Anne de Bellevue, Québec,
20 H9X 3V9, Canada. Tel: (+1) 514-398-7920, Email: saji.george@mcgill.ca



21 **Abstract**

22 Bovine mastitis (BM), resulting from intramammary infection, is one of the costliest diseases
23 in animal agriculture. Occasional treatment failure and bacterial persistence in the mammary gland
24 demand alternate therapeutic approaches. Nanotechnology-enabled Antibacterial Combination
25 Therapy (NeACT), which utilizes nanomaterials to co-deliver more than one drug molecule with
26 synergistic and complementary antibacterial mechanisms, holds promise for BM treatment. Here,
27 we developed a NeACT constituting ceftiofur(CF) loaded chitosan nanoparticles conjugated with
28 chlorpromazine(CPZ) and tannic acid(TA) loaded cyclodextrin nanoparticles. CF, CPZ, and TA
29 showed a synergistic antibacterial action ($FICI=0.49$) against a methicillin-resistant *Staphylococcus*
30 *aureus* strain (Sa1158c) isolated from BM. NeACT demonstrated colloidal stability,
31 biocompatibility, and slow-release of payloads and showed a significant reduction in Sa1158c efflux
32 pump (by ~15.53-fold) and biofilm-forming (by ~3.40 \log_{10}) abilities. It showed low
33 immunogenicity and no adverse effect on the mammary tissues of CD-1 lactating mice in a mastitis
34 model. NeACT of ≥ 3.90 $\mu\text{g}/\text{mL}$ demonstrated ≥ 3.20 \log_{10} reduction of internalized Sa1158c in
35 epithelial cells *in vitro*, while NeACT of 39 $\mu\text{g}/\text{gland}$ showed ≥ 4.46 \log_{10} remediation of Sa1158c
36 from infected mice. Overall, NeACT successfully reduced the effective concentration of CF, CPZ,
37 and TA and overcame Sa1158c CF resistance. These desirable therapeutic characteristics warrant
38 its application for treating BM.

39

40 **Keywords:** bovine mastitis, intramammary infection, methicillin-resistant *Staphylococcus aureus*
41 (MRSA), Nano-enabled Antibacterial Combination Therapy (NeACT), antimicrobial resistance,
42 animal agriculture, murine mastitis model



44 **1. Introduction**

45 Bovine mastitis (BM) is the inflammation of the mammary gland tissues, primarily resulting
46 from an intramammary infection (IMI)¹. Owing to reduced milk production, milk loss, treatment
47 failures, *etc.*, the yearly financial loss in some prominent milk-producing countries such as the
48 United States, Canada, and India amounts to \$2 billion, \$310 million, and \$971 million, respectively,
49 making BM the most threatening bacterial disease in the dairy cattle industry¹. Out of several
50 contagious pathogens, *Staphylococcus aureus* is one of the most prevalent organisms associated
51 with BM, accounting for almost 40-70% of the cases globally². *S. aureus* colonizes tissues lining
52 the milk-collecting spaces and induces weak inflammation and host immune responses¹. This ability
53 in *S. aureus* is predominant in their persistence and chronic infection¹.

54 The treatment of BM often involves intramammary infusion or parental administration of
55 antibiotics to dairy cows during lactation or the dry period¹. According to the United States
56 Department of Agriculture (USDA), cephalosporins (53.2%), lincosamide (19.4%), and non-
57 cephalosporin β-lactam antibiotics (19.1%) are the most common antibiotics in use to treat BM³.
58 Non-selective blanket antimicrobials used as prophylactic control often impart selective pressure on
59 mastitis pathogens such as *S. aureus*, leading to antimicrobial resistance (AMR)⁴. Such pathogens
60 may possess intrinsic or acquired resistance mechanisms that could limit drug uptake,
61 inactivate/modify a drug, and show virulence, such as biofilm formation, hemolysin production,
62 intracellular survivability, *etc.*, contributing to treatment failures⁵⁻⁷. Indeed, the cure rate of *S.*
63 *aureus*-mediated mastitis in cows with intramammary treatment during lactation or at dry-off rarely
64 exceeds 50%⁸. The prevalence of AMR among mastitis pathogens is rising, evidenced by the
65 increasing resistance rate towards crucial antibiotics such as beta-lactams and cephalosporins,
66 between 30-70% in the USA and more than 85% in Ireland and Brazil⁹. Vaccines against *S. aureus*



67 *in* BM, namely Lysigin® in the USA and Startvac® in Europe and Canada, failed to provide
68 significant protection against reinfection^{10, 11}. Overall, these challenges warrant cost-effective,
69 sustainable alternate strategies that are efficient in BM treatment.

70 Antibacterial combination therapy is defined as '*combining antibiotic/s and/or adjuvant*
71 *molecules with synergistic properties to improve antibacterial treatment outcomes*'¹. The
72 mechanism of such a combination involves common or complementary interactions, including
73 sequential inhibition of the same biochemical pathway, inhibition of bacterial antimicrobial-
74 modifying enzymes, *etc.*¹²⁻¹⁴. Although combination therapy has been employed in biomedical and
75 agricultural sectors, poor drug bioavailability, retention rate, cytotoxicity, stability, and overdosing
76 have restricted its widespread acceptance¹. We believe that nanotechnology-enabled approaches
77 could resolve these issues. The nano size and multifunctionality of nanomaterials provide
78 unprecedented advantages for the targeted delivery of drugs across biological barriers^{1, 15}. We term
79 this strategy as Nano-enabled Antibacterial Combination Therapy (NeACT) and define it as '*the*
80 *therapeutic strategy aimed at harnessing the power of a nano-delivery platform to deliver more than*
81 *one drug molecule with complementary function for effective antibacterial treatment*'¹.

82 In this study, we selected ceftiofur (CF), a cephalosporin, as the primary antibiotic for
83 combination therapy. Although CF is extensively used in subclinical BM, it could have a cure rate
84 as low as 0% against *S. aureus*^{8, 16, 17}. Chlorpromazine (CPZ) and a polyphenol, Tannic acid (TA),
85 were selected as adjuvants as they complement the action of CF by inhibiting bacterial efflux pumps,
86 disrupting biofilms and membrane integrity¹⁸⁻²⁰. Chitosan (CH) is a polysaccharide widely used in
87 nanomedicine because of its desirable characteristics for drug delivery, such as cationic charge,
88 biocompatibility, low toxicity, low immunogenicity, ability to adhere to mucosal surfaces, and
89 improved permeability of macromolecules through the epithelial tight junction²¹. CH nanoparticles



have been reported to exhibit prolonged residence time at drug absorption sites, enabling higher drug penetration and targeting intracellular pathogens, thus being suitable as a single drug carrier in complex IMI environments, meriting their application as a carrier for CF²¹. The hydroxypropyl derivatives of β -cyclodextrin (CD) are biocompatible cyclic oligosaccharides containing a relatively hydrophobic central cavity and hydrophilic outer surface²². CD has been reported to improve solubility and enhance drug stability, drug molecule permeability, and bioavailability²². It can encapsulate or adsorb multiple payloads due to its hydrophobic central cavity and hydrophilic outer surface. Therefore, we selected CD as a carrier for CPZ and TA. Overall, we designed a unique nanocomposite constituting CF-loaded CH nanoparticles conjugated with CPZ and TA-loaded CD nanoparticles (hereafter referred to as NeACT). NeACT was tested under an *in vitro* system to understand its mechanism of action against pathogens. Further, its ability to remediate an IMI caused by a methicillin-resistant *Staphylococcus aureus* strain isolated from BM was verified successfully using the lactating mouse mastitis model.

103

104 **2. Materials and methods**105 **2.1. Reagents and chemicals**

106 The (2-Hydroxypropyl)- β -cyclodextrin (CD) (molecular weight: ~1396 Da) (product
107 number: H107), Chitosan (85% deacetylated) (CH) (medium molecular weight) (product number:
108 448877), Tannic acid (TA) (molecular weight: 1701.20) (product number: 16201), Chlorpromazine
109 (CPZ) (molecular weight: 355.33) (product number: C8138), Ceftiofur (CF) (molecular weight:
110 523.56) (product number: 34001), Sodium tripolyphosphate (TPP), Mueller–Hinton Broth (MHB),
111 Dimethyl sulfoxide (DMSO), Resazurin sodium salt, Nylon filter membranes (of 0.22 μ m and 0.45
112 μ m), Insulin, Hydrocortisone, Poly-L-lysine, Fluorescein isothiocyanate (FITC), Glutaraldehyde



113 solution, and Ethidium bromide (EtBr) were purchased from Sigma-Aldrich, Canada. The 32-gauge
114 blunt needles were purchased from TSK Laboratory International, Canada. Gibco Dulbecco's
115 Modified Eagle Medium (DMEM), Hoechst 33342, Propidium iodide (PI), Probe-On Plus slides,
116 and Sterile petri dishes were purchased from ThermoFisher, Canada. Fetal bovine serum (FBS) was
117 purchased from Wisent, Canada. Gentamicin sulfate was purchased from Bio Basic, Canada. Human
118 colorectal adenocarcinoma (Caco-2) cells were purchased from ATCC, USA. The quality control
119 (QC) strain *Staphylococcus aureus* ATCC 25923 was purchased from Oxoid Company, Canada.
120 The methicillin-resistant *S. aureus* strains Sa1158c (Isolate ID: 10812464, Accession no. NCBI:
121 SRR11471981) and Sa30 (Isolate ID: 21000024, Accession no. NCBI: JAANBF00000000) were
122 collected from the Canadian mastitis pathogen culture collection (MPCC) ⁷. CD-1 lactating mice
123 were purchased from Charles River Laboratories, Canada.

124

125 **2.2. Assessment of CF, CPZ, and TA for antibacterial synergism**

126 A three-dimensional checkerboard assay, as previously described by Stein *et al.*, was
127 conducted to assess the antibacterial efficiency of the combination (CF, TA, and CPZ) ²³. More
128 information on the checkerboard assay is provided in **Supplementary information 1**.

129

130 **2.3. Synthesis of CPZ and TA-loaded CD nanoparticles (CPZ-CD-TA)**

131 A 6:6:6 mM ratio of CD, TA, and CPZ was used for CPZ-CD-TA preparation. Briefly, 138.6
132 mg of CD was dispersed in 3 mL of ethanol and sonicated for 10 mins. The resulting suspension
133 was added dropwise to a solution of CPZ (28.62 mg) in 10 mL of DI water under constant stirring.
134 CPZ-CD was sonicated for 15 mins, and a 2 mL ethanol solution containing 153.09 mg of TA was
135 added dropwise. CPZ-CD-TA was kept under constant stirring for 5 hours at 40 °C and then under



136 vacuum for 30 mins. Subsequently, the solution was filtered using a 0.45 μ m nylon filter membrane
137 to remove the unreacted agents and residual impurities. CPZ-CD-TA was refrigerated at -20 °C and
138 lyophilized using a freeze dryer (FreeZone 12L-50C, Labconco Corp., USA). The dried sample was
139 stored in a desiccator for future use.

140

141 **2.4. Synthesis of CPZ-CD-TA conjugated CF-loaded CH nanoparticles (CH Np-CF(CPZ-CD-
142 TA) or NeACT)**

143 CH (2 mg/mL) was added to DI water, dissolved by adding acetic acid (final concentration
144 of 1%), and stirring the solution for 48 h. Subsequently, the pH was raised to 4.7-4.8 using 1 N
145 NaOH. CF (1.5 mg/mL) was dissolved in DI water and added to the CH solution dropwise. The
146 resulting mix was stirred for 15 mins and sonicated for another 15 mins. TPP, at a concentration of
147 1/3rd of CH, was added dropwise to the solution under constant stirring to form CH Nps entrapping
148 CF. The formed CH Np-CF was stirred for 30 mins, sonicated for 15 mins, and stirred for another
149 1 h. The sample was centrifuged (7500 \times g for 10 mins) (Sorvall Instruments, Thermo Fisher
150 Scientific, USA), washed, and resuspended in PBS. Freeze-dried CPZ-CD-TA was added to the
151 PBS buffer and dispersed with sonication and vigorous stirring. CH Np-CF was added dropwise to
152 the solution at a 3:1 ratio (CPZ-CD-TA: CH Np-CF) and stirred for 4 h to allow fusion between the
153 two entities through electrostatic interaction. The CH Np-CF(CPZ-CD-TA), referred to as NeACT,
154 was washed thrice, resuspended in PBS, and stored at 4 °C for further analysis.

155

156 **2.5. Fluorescein isothiocyanate (FITC) labeling of NeACT**



157 As-synthesized NeACT (10 mg/mL) was added with FITC (1 mg/mL, dissolved in DMSO) at
158 room temperature and incubated under vigorous stirring in the dark for 12 h. The FITC-labeled
159 NeACT (FITC-NeACT) was centrifuged ($7,500 \times g$ for 10 mins) and washed thoroughly with sterile
160 DI water until no color or residue was observed in the supernatant. Fluorescence images of particles
161 were taken using an automated epi-fluorescence microscope (Cell Discoverer 7, Carl Zeiss,
162 Germany) to confirm the labeling of NeACT with FITC.

163

164 **2.6. Physicochemical characterization of the particles**

165 Attenuated total reflectance-Fourier transform infrared (ATR-FT-IR), Scanning Electron
166 Microscope (SEM), and Dynamic Light Scattering (DLS) analysis were used to assess the surface
167 functional groups, surface morphology, and hydrodynamic size and surface charge of the particles,
168 respectively. More information on the physicochemical characterization of the particles is provided
169 in **Supplementary information 2**.

170

171 **2.7. Loading capacity of particles and release profile of CF, CPZ, and TA**

172 The loading capacity of the particles and release profile of the drug molecules (CPZ, TA,
173 and CF) were determined using a Varian ProStar HPLC system (Varian, USA) equipped with a
174 Gemini-NX 5u C18 110A column (100×4.60 mm, 5 μm particle size, Phenomenex, USA). For
175 this, NeACT particles (1 mg/mL) were centrifuged ($31,000 \times g$ for 20 mins) (Sigma 3-30 KHS,
176 Germany), as centrifugation at high RPM could disrupt the polymeric matrix to release the contents
177 ²⁴. The supernatants were filtered using a 0.22 μm nylon filter membrane. A 20 μL of the supernatant
178 was injected into the chromatographic system. The mobile phase consisted of methanol-acetonitrile-
179 acetic acid (5%) in a volume ratio of 6:7:87 at a 1.2 mL/min flow rate. The detection wavelengths



180 for CPZ, TA, and CF were 306 nm, 280 nm, and 292 nm, respectively. The availability (amount of
181 payload contained by nanocarrier) of CPZ, TA, and CF in NeACT was subsequently determined
182 from a standard curve (concentration range: 1 mg/mL–0.05 mg/mL).

183 The loading capacity was determined following Equation 1.

184
$$\% \text{ Loading capacity} =$$

185
$$(\text{Concentration of 'X' in supernatant after centrifuging NeACT} \div \text{Initial concentration of 'X' added to NeACT}) \times 100$$
 ..(Equation 1)

187 where 'X' is CF, CPZ, or TA.

188 To determine the release profiles of CPZ, TA, and CF from NeACT as a function of time,
189 a 1 mg/mL NeACT suspension was prepared in 10 mL of PBS buffer, supplemented with 10% FBS
190 (pH 7.4) to mimic the bovine mammary microenvironment. The suspension was incubated at 37 °C
191 under minimal shaking at 100 rpm. One milliliter of NeACT was gently centrifuged (3,000 × g for
192 1 min), and the supernatant was collected every 24 hours for a period of seven days. The supernatant
193 was filtered, and the HPLC was used to quantify CF, CPZ, and TA in the supernatant as detailed
194 above. The percentage of payload release as a function of time was determined following Equation
195 2.

196
$$\% \text{ Payload release} =$$

197
$$(\text{Concentration of 'X' in supernatant each day of sample collection} \div \text{Initial concentration of 'X' in NeACT}) \times 100$$
 ..(Equation 2)

199 where 'X' is CF, CPZ, or TA.

200

201 2.8. *In vitro* antibacterial efficiency of particles

202 The *in vitro* antibacterial efficiency of the particles was determined using a broth
203 microdilution method²⁵. More information on this method is provided in **Supplementary**
204 **information 3**.



205 The effect of particles on bacterial membrane integrity was assessed using a PI dye uptake
206 assay¹². As detailed earlier, the particles (125 µg/mL) were subjected to ten-twofold serial dilution
207 in 100 µL of MHB media in a 96-well plate. Ten µL of the culture maintained at a 0.5 McFarland
208 standard was added to the wells and incubated for 6 h at 37 °C. PI dye (3.34 µg/mL) suspended in
209 PBS was added to the wells and incubated for 30 mins. The fluorescence intensity was measured at
210 an excitation/emission wavelength of 555/645 nm using a plate reader (SpectraMax-i3X, Molecular
211 devices, USA) to assess PI uptake into cells with compromised membranes.

212 SEM was used to assess changes in the morphological features of bacteria after
213 being exposed to NeACT²⁶. Briefly, bacterial culture maintained at 0.5 McFarland standard was
214 subjected to a sub-lethal concentration (1.95 µg/mL or half of MIC value against Sa1158c) of
215 NeACT and incubated for 6 h at 37 °C with gentle shaking. Bacterial cells were harvested by
216 centrifugation (4,000 × g, 3 mins) and washed twice with PBS (1X, pH 7.4). The washed cells were
217 fixed using 2.5% glutaraldehyde at 4 °C for 2 h. Fixed cells were dropped onto poly-l-lysine-coated
218 coverslips and subjected to serial dehydration by exposing them to incremental concentrations of
219 ethanol (20-100%). Further, these cells were subjected to critical point drying (Leica EM CPD300,
220 Germany) and were used for SEM examination after sputter coating with Platinum. ImageJ software
221 was used to measure the size of bacterial cells.

222

223 **2.9. Efficiency of NeACT against resistance mechanisms of *S. aureus***

224 The anti-efflux activity of NeACT was measured using a pre-established EtBr assay¹⁴.
225 Briefly, bacterial cultures maintained at 1.0 McFarland standard (3×10^8 cells/mL) were treated
226 with sub-lethal concentrations (1/3rd of MIC value against Sa1158c) of NeACT (1.30 µg/mL) and
227 control groups (CH Np-CF (20.83 µg/mL) and CPZ-CD-TA (83.33 µg/mL)). The suspension was
228 vortexed and incubated at 37 °C for 30 min. A sub-lethal concentration of EtBr (0.65 µg/mL or 1/3rd



of the MIC value against Sa1158c) was added further to the suspension and incubated for another 30 min. Bacterial cells were washed, re-suspended in PBS (1X, pH 7.4), and transferred (140 μ L) to a 96-well plate. EtBr efflux was triggered by glucose (10 μ L; final concentration 0.1% w/v), and efflux activity was determined by monitoring the increase in fluorescence intensity (530/590 nm) for 60 min using a plate reader. Sa1158c, without particle exposure, was considered a positive control, while Sa25923, with no efflux pump activity, was used as a negative control. GraphPad Prism 7 software was used to determine the time-dependent efflux of EtBr using a single exponential decay equation, as detailed previously ⁶. The time taken for the bacterial cells to extrude 50% of EtBr was denoted as $t_{\text{efflux}50\%}$.

For assessing the antibiofilm property of NeACT ¹², 200 μ L of TSB media suspended with incremental concentrations (0.24-125 μ g/mL) of NeACT and control particles in a 96-well plate were added with 20 μ L of the Sa1158c culture adjusted to 0.5 McFarland standard. After 48 h of incubation, the media were removed from the wells, and the wells were washed with sterile PBS. Subsequently, 100 μ L of 99% methanol was added, and the plates were kept undisturbed for 15 min. Methanol was removed from the wells, and 200 μ L of CV solution (0.4%) was added. The plates were incubated for 2 h, washed, and 100 μ L of acetic acid (33%) was added. The biomass of the biofilms was quantified by measuring the absorbance values at 570 nm using a plate reader.

The viability of Sa1158c cells present in biofilm was assessed after treating with increasing concentrations (0.24-125 μ g/mL) of the particles. Briefly, 10 μ L of Sa1158c isolate maintained at 0.5 McFarland standard was added to 100 μ L of TSB media in a 96-well plate. The plate was incubated for 24 h to allow biofilm formation, followed by the addition of NeACT and control particles. The plate was incubated for another 24 h at 37 °C. The 100 μ L of TSB media was discarded without damaging the biofilm. Subsequently, 100 μ L of PBS was added to the wells containing



252 biofilms, and the biofilm cells were suspended by vigorous pipetting. The CFU was enumerated
253 using the drop plate culturing method, as detailed in **Supplementary information 3**.

254 To visualize the penetration of NeACT into the biofilm matrix, a fluorescent-labeled Sa30
255 isolate was obtained by introducing plasmid pSRFPS1 (coding red fluorescence protein (RFP))⁷
256 was used. Ten μ L of RFP labeled Sa30 isolate (maintained at 0.5 McFarland standard) was
257 incubated for 24 h (at 37 °C) in a 96-well plate containing 100 μ L of TSB media to allow biofilm
258 formation. FITC-NeACT (20.83 μ g/mL or 1/3rd of the MIC value against Sa30) was exposed to the
259 biofilms and incubated further for 24 h. Subsequently, 100 μ L of the TSB media was discarded, and
260 100 μ L of PBS was added to the wells. Fluorescence images of the biofilms (Red fluorescence
261 imaged using a 583 nm filter) and FITC-NeACT (Green fluorescence imaged using a 519 nm filter)
262 were captured at 20X magnification using an epifluorescence high content microscope (Cell
263 Discoverer 7). 3D images were constructed by stacking images captured from different depths.

264

265 **2.10. Efficiency of NeACT against internalized *S. aureus* in epithelial cells**

266 The cytotoxicity of NeACT was tested in Caco-2 cells. The efficiency of NeACT in targeting
267 internalized *S. aureus* in epithelial cells (Caco-2) was also determined. More information on the
268 method is provided in **Supplementary information 4**.

269

270 **2.11. Efficiency of NeACT in a murine model of mastitis**

271 The institutional ethics committee on animal experimentation of the Faculté des Sciences of
272 the Université de Sherbrooke (QC, Canada) approved the *in vivo* experiments, and the guidelines of
273 the Canadian Council on Animal Care were respected during all procedures.



274 CD-1 lactating mice were separated from their pups (12-14 days following birth) and
275 anesthetized using isoflurane ²⁷. The fourth pair of glands, found from head to tail (L4 and R4
276 glands), was first disinfected with 70% ethanol for inoculation. A 100 μ L of PBS containing 100-
277 125 CFUs of Sa1158c was slowly injected into the lactiferous duct with a 32-gauge blunt needle
278 attached to a 1 mL syringe. Four hours post-inoculation, mice were anesthetized again, and
279 incremental concentrations of NeACT (20 (78 μ g/gland), 10 (39 μ g/gland), and 5 (19.5 μ g/gland)
280 times of *in vitro* MIC value against Sa1158c) were injected directly into the mammary glands
281 previously infected (6 mammary glands: n=6). Similarly, CH Np, CD, CH Np-CF, and CPZ-CD-
282 TA (working concentration: 78 μ g/gland or 20 times of *in vitro* NeACT MIC value against Sa1158c)
283 were used as control particles and were injected into the infected mammary glands (6 mammary
284 glands per control group). Hundred μ L of PBS used as the media control was injected into eight
285 infected mammary glands (n=8). Each infected gland was considered as an experimental unit. After
286 14 h of bacterial inoculation, mice were anesthetized and humanely euthanized, mammary glands
287 were harvested, and one set was homogenized for measuring bacterial count; the other set was kept
288 for histological studies (see section 2.12). CFU counts were obtained after plating a serial dilution
289 of mammary gland homogenates on TSA petri dishes that were incubated at 37 °C for 24 h. The
290 detection limit was approximately 200 CFU per gram of mammary glands.

291

292 **2.12. Tissue preparation and histological studies**

293 Mammary glands from the NeACT-treated and untreated mice were fixed in 4% PFA
294 overnight at 4°C, dehydrated in 70% ethanol to avoid adipose distortion, and embedded in paraffin
295 ²⁸. Subsequently, the paraffin blocks were incubated at -20 °C for 1 h. Tissue sections of 5 μ m were
296 cut using a microtome (Shandon Finesse ME+ paraffin sectioning microtome, GMI, USA), applied



297 to Probe-On Plus slides, and kept at room temperature. Hematoxylin and Eosin Y (H&E) staining
298 and Masson's trichrome staining were performed to investigate immune responses
299 and morphological and cellular alterations in infected and NeACT-treated mammary glands, while
300 Gram staining was performed to stain and detect Sa1158c in infected mammary tissues. H&E and
301 Masson's trichrome staining was conducted on an automated platform (Shandon varistain 24-4 slide
302 stainer, GMI, USA). Tissue preparation, embedding, and coloration (H&E, Masson's trichrome, and
303 Gram staining) were performed by the Electron Microscopy and histology platform at the Université
304 de Sherbrooke²⁷. Images were captured on a Nanozoomer Digital Slides Scanner (Hamamatsu,
305 Japan).

306

307 **2.13. Statistical analysis**

308 *t*-test and one-way ANOVA were performed as required to check the statistical significance,
309 wherein a *p*-value ≤ 0.05 was considered significant. 'GraphPad Prism 7' software was used to
310 perform the statistical analysis.

311

312 **3. Results**313 **3.1. Checkerboard assay**

314 The checkerboard assay assessed the combinatorial effect of the CF, CPZ, and TA against
315 Sa1158c. An FICI of <0.8 was considered a synergistic relationship among the combinations. The
316 MICs of CF, CPZ, and TA against Sa1158c were 31.25, 500, and 500 $\mu\text{g}/\text{mL}$, respectively. Notably,
317 the CLSI breakpoint for CF is $\geq 8 \mu\text{g}/\text{mL}$, suggesting CF resistance by Sa1158c. When CF, CPZ,
318 and TA were combined, the MICs were reduced significantly by 8-fold (MIC: 3.91 $\mu\text{g}/\text{mL}$), 4-fold



319 (MIC: 125 μ g/mL), and 8-fold (MIC: 62.5 μ g/mL), respectively. The FICI for combinations of CF,
320 CPZ, and TA was 0.49, indicating a synergistic interaction.

321

322 3.2. Physicochemical characterization of the particles

323 The FTIR spectra of NeACT is provided in **Figure 1a**. In NeACT, CH Np-CF was evident
324 from the peaks at 2938 and 2892 cm^{-1} (stretching vibrations of methylene groups), 1065 cm^{-1} (C-O-
325 C stretching vibrations), 1526 cm^{-1} (-NH₂ bending vibration peak), 1026 cm^{-1} (P=O stretching
326 vibration), 1759 cm^{-1} (C=O stretching), 1382 cm^{-1} (C-N stretching), and 1690 cm^{-1} (thioester group).
327 The signals at 859 cm^{-1} (α -type glycosidic bond), 2938 cm^{-1} (C-H stretching vibration), 1187 cm^{-1}
328 (O-H bending), 1442-1705 cm^{-1} (benzene rings), 1607 cm^{-1} (phenyl rings), 756 cm^{-1} (aromatic C-H
329 bending) corresponded to the functional groups of CPZ-CD-TA in NeACT. The shifts in FTIR
330 spectra in the case of NeACT indicate hydrogen bonding formation due to the interactions between
331 the payloads and the nanocarriers. More details on the functional groups associated with CPZ-CD-
332 TA and CH Np-CF are provided in **Supplementary information 2**.

333 SEM analysis revealed the morphology of the particles (**Figures 1b-g**). CPZ-CD-TA
334 conjugated with CH Np-CF through electrostatic interactions to develop NeACT and ranged
335 between \sim 250-400 nm. The hydrodynamic sizes of CH Np, CH Np-CF, and NeACT were \sim 269,
336 \sim 309, and \sim 539 nm, respectively. The zeta potential for CH Np and CH Np-CF ranged between
337 +28-30 mV, which, however, reduced to \sim +21.6 mV in the case of NeACT, indicating the
338 electrostatic interaction between CH Np-CF and CPZ-CD-TA (**Table 1**). Indeed, a zeta potential
339 close to +30 mV suggests sufficient repulsive forces and superior physical colloidal stability ¹².
340 More information on the SEM and DLS analysis associated with CD Np, CH Np, CPZ-CD-TA, and
341 CH Np-CF is provided in **Supplementary information 2**.



342

343 **3.3. Loading capacity of NeACT and release profile of CF, CPZ, and TA**

344 The loading capacity of NeACT for the payloads was determined using HPLC. The
345 availability (amount of payload contained in nanocarrier) of CF, CPZ, and TA in 1 mg/mL of
346 NeACT was ~32.14%, ~18.78%, and ~16.85%, respectively (**Figure 2a**). The availability of CF in
347 1 mg/mL of CH CF-Np was 44.66%, while the loading capacity of CD Np (1 mg/mL) for CPZ and
348 TA were 26.88% and 25.78%, respectively. The release profile of NeACT was monitored every 24
349 h for 7 days in PBS buffer supplemented with 10% FBS (pH 7.4). The release of 50% CF, CPZ, and
350 TA from 1mg/mL of NeACT was observed between the 2nd and 3rd day, while a 100% release was
351 seen by the 7th day (**Figure 2b**).

352

353 **3.4. *In vitro* antibacterial efficiency and mechanism of action of NeACT**

354 NeACT showed excellent antibacterial properties against the tested bacteria, Sa1158c and
355 Sa25923. For instance, the MIC for NeACT against Sa25923 and Sa1158c were 0.48 μ g/mL and
356 3.91 μ g/mL, respectively. NeACT showed a \sim 7.05 \log_{10} Sa25923 reduction and \sim 7.51 \log_{10} Sa1158c
357 reduction ($p<0.05$) at the MIC (**Figure 3a and 3b**). On the contrary, CF, CPZ, TA, CPZ-CD-TA,
358 and CH Np-CF at the same concentrations showed no significant difference ($p>0.05$) from the
359 control group (Sa25923 and Sa1158c without treatment). The MIC for CPZ-CD-TA and CH CF-
360 Np against Sa1158c was 250 and 62.5 μ g/mL, respectively. The MICs for pristine CF, CPZ, and
361 TA were 31.25, >250, and >250 μ g/mL, respectively, against Sa1158c. Interestingly, the availability
362 of CF, CPZ, and TA in NeACT at its MIC (3.91 μ g/mL) against Sa1158c was 1.25, 0.73, and 0.65
363 μ g/mL, respectively (based on the loading capacity of NeACT), suggesting a significant decrease

364 in the effective concentration of CF (by 25-fold), CPZ (by >342-fold), and TA (by >384-fold) than
365 their pristine form. This superior performance of NeACT was owed to the synergistic effect of the
366 combination.

367 The effect of NeACT on bacterial membrane integrity was measured by PI uptake assay
368 (**Figure 3c**). NeACT showed significant damage to the Sa1158c membrane. For instance, at 3.91
369 $\mu\text{g/mL}$, a ~8.85-fold increase ($p<0.05$) in PI fluorescence was observed, suggesting a compromised
370 Sa1158c membrane. The rate of damage increased with increasing concentrations of NeACT.
371 Compared to the control group (bacteria with no treatment), CPZ-CD-TA at 62.5 $\mu\text{g/mL}$ and CH
372 Np-CF at 31.25 $\mu\text{g/mL}$ showed ~2.74 and ~8.03-fold increase in PI fluorescence, respectively.
373 **Figures 3d and 3e** represent Sa1158c cells before and after exposure to 1.95 $\mu\text{g/mL}$ of NeACT.
374 Ruptured membrane and corrugated morphology with wrinkles and cracks were evident in NeACT-
375 treated Sa1158c cells due to the loss of membrane integrity²⁹.

376 Sa1158c cells extruded 50% of the EtBr molecules ($t_{\text{efflux}50\%}$) in only 94.10 secs, while the
377 exposure (1/3rd of MIC value against Sa1158c) of CPZ-CD-TA (at 83.33 $\mu\text{g/mL}$), CH Np-CF (at
378 20.83 $\mu\text{g/mL}$), and NeACT (at 1.30 $\mu\text{g/mL}$) reduced the extrusion rate significantly ($p<0.05$) by
379 >38.25-fold, ~6.63, and ~15.53-fold, respectively, suggesting the efflux inhibition property of the
380 particles (**Figures 3f and 3g**). It was evident that CPZ-CD-TA has contributed to the efflux
381 inhibition property in NeACT.

382 The ability of NeACT to restrict biofilm formation was verified (**Figure 4a**). CPZ-CD-TA,
383 CH Np-CF, and NeACT inhibited 50% biofilm formation at 9.73, 69.14, and 0.45 $\mu\text{g/mL}$,
384 respectively. While CPZ-CD-TA reduced Sa1158c biofilms by ~3.18 \log_{10} at 125 $\mu\text{g/mL}$, NeACT
385 (at 3.91 $\mu\text{g/mL}$), and CH Np-CF (at 62.5 $\mu\text{g/mL}$) showed ~3.38 \log_{10} and ~3.70 \log_{10} reduction,
386 respectively (**Figure 4b**). To investigate the penetration and accumulation of FITC-labelled NeACT



387 (coding green), a sub-lethal dosage (20.83 μ g/mL or 1/3rd of FITC-NeACT MIC value against Sa30)
388 was subjected to the biofilms of RFP-tagged Sa30 (coding red). Compared to untreated control, a
389 significant reduction in biofilm biomass was evident (**Figure 4c-f**). Moreover, Z-stack images
390 suggested the accumulation and penetration of NeACT in Sa30 biofilms (**Figure 4e-f**).

391

392 **3.5. Efficiency of NeACT against internalized *S. aureus* in epithelial cells**

393 The efficiency of NeACT against internalized pathogens was examined in a Caco-2 cell
394 model of intracellular infection, where the Caco-2 cell line was used as a representative model
395 epithelial cell line. No cytotoxicity was detected for the tested particles (NeACT, CH CF-Np, CPZ-
396 CD-TA, CH Np, and CD Np) in Caco-2 cells, as 100% viability was observed at 250 μ g/mL of the
397 particles (**Figure 5a**) (the highest dose tested). NeACT showed a significant reduction in
398 intracellular Sa1158c (**Figure 5b**). For instance, at the MIC value of 3.9 μ g/mL, NeACT showed a
399 3.27 \log_{10} reduction ($p<0.05$) of internalized Sa1158c from the Caco-2 cells. Similarly, at 7.81 and
400 15.62 μ g/mL, NeACT reduced intracellular Sa1158c colonization by 4.49 \log_{10} and 7.01 \log_{10} ,
401 respectively.

402

403 **3.6. *In vivo* efficiency of NeACT on CD-1 mice model of mastitis infection**

404 CD-1 lactating mice were used as a mastitis infection model to evaluate NeACT efficiency.
405 A 7.4 \log_{10} Sa1158c CFU/g of tissue was detected from mammary glands without treatment (**Figure**
406 **5c**). As expected, CPZ-CD-TA had no effect on Sa1158c inhibition, while CH Np-CF (at 78
407 μ g/gland) showed a significant \sim 3.44 \log_{10} Sa1158 reduction. NeACT showed a superior ($p<0.05$)
408 remediation of Sa1158c from the mammary gland compared to all control groups. For instance, a



409 low dose of 78 $\mu\text{g}/\text{gland}$ and 39 $\mu\text{g}/\text{gland}$ of NeACT showed $\sim 5.13 \log_{10}$ ($>99.999\%$) and ~ 4.46
410 \log_{10} ($>99.99\%$) *Sa1158c* reduction, respectively, from mice mammary gland.

411 H&E and Masson's trichrome staining were performed on mammary tissues to examine
412 PMN infiltration, morphological, and cellular alterations. No inflammation and negligible PMN
413 infiltration (as the large dark purple spheres with a multi-lobular nucleus, indicated with black
414 arrows in **Figure 6a-d**) or lesions in the supportive connective tissue were observed in the untreated
415 noninfected tissues and NeACT-treated noninfected tissues. Adipocytes (indicated with red arrows
416 in **Figure 6a-h**) were evident in all the tissues as signet-shaped cells, with a nucleus at the periphery,
417 with visible fat droplets, and a thin layer of cytoplasm. The pink staining within the alveoli
418 represented milk components ³⁰. Compared to NeACT-treated infected tissues, collapsed alveoli
419 and necrotic areas were detected in untreated infected tissues. Moreover, PMN infiltration (indicated
420 with black arrows in **Figure 6e-h**) was significantly evident in the connective tissue and intraluminal
421 space of the untreated infected tissues.

422

423 4. Discussion

424 We designed and tested a novel Nano-enabled Antibacterial Combination Therapy (NeACT)
425 comprised of ceftiofur (CF)-loaded chitosan nanoparticles (CH Np) conjugated with
426 chlorpromazine (CPZ) and tannic acid (TA)-loaded cyclodextrin nanoparticles (CD Np). NeACT
427 demonstrated exceptional colloidal stability, biocompatibility, and slow-release properties of the
428 payloads. The synergistic interaction of components used in NeACT resulted in a dramatic decrease
429 in bacterial load in a mouse model of mastitis.



430 Previously, our group reported the characterization of a library of *S. aureus* strains isolated
431 from bovine mastitis for antibiotic resistance and virulence traits⁷. In that study, we identified
432 Sa1158c as an MDR MRSA strain resistant to CF (the antibiotic used in this study)⁷. Studies have
433 reported that the cure rate of MDR *S. aureus* infection by CF could be around 47% but could get as
434 low as 0%^{8, 16, 17}. As anticipated, we observed a synergistic action among CF, CPZ, and TA. This
435 is ascribed to the complementary mode of action of the selected antibiotic-adjuvant combination (as
436 discussed later).

437 We examined the release profile of CF, CPZ, and TA from NeACT every 24 h for seven
438 days. A 50% release of all the payloads was observed within 2-3 days. The release of CPZ and TA
439 from CD Np is probably through dilution-mediated dissociation³¹, while the release of CF from CH
440 Np is probably through diffusion or shrinkage, causing release due to attractive electrostatic
441 interaction between anions and chitosan matrix at a higher pH^{32, 33}. Compared to previous studies
442 that reported a much faster release of drugs (within 6 to 12 h) from polymeric nanoparticles³², our
443 observations suggested a slow-release behavior of payloads from the nanocarriers. One of the most
444 significant drawbacks of CF is its elimination before 12 h after intramammary infusion, as it gets
445 rapidly metabolized³⁴. The slow release of payloads from NeACT could contribute significantly to
446 improving the retention time of CF in the mastitis microenvironment.

447 NeACT showed excellent antibacterial efficiency *in vitro* against Sa1158c at a dosage of 3.9
448 µg/mL. Based on the loading capacity of NeACT, the amounts of CF, CPZ, and TA contained in
449 3.91 µg/mL of NeACT were 1.25, 0.73, and 0.65 µg/mL, respectively. Previous studies from our
450 group reported that Sa1158c possesses efflux pump activity, beta-lactamase enzyme production,
451 and strong biofilm-forming ability⁷. Genomic studies revealed genes associated with major
452 facilitator superfamily (MFS) efflux pumps (*norA*, *norB*, *tetM*, etc.), cephalosporin resistance (*blal*,



453 *blaR*, *blaZ*, *mecA*, etc.), and fibronectin-binding proteins (*fnbA*, *fnbB*, etc.), underpinning efflux
454 activities⁷. Therefore, the efficiency of NeACT was tested against these resistance mechanisms.
455 The increase in PI fluorescence suggested that NeACT disrupted the *Sal1158c* cell membrane.
456 Interestingly, a significant increase in width was noticed among the *Sal1158c* cells under NeACT
457 stress. Cell wall-targeting antibiotics, such as CF, bind to penicillin-binding proteins (PBPs) and
458 inhibit peptidoglycan synthesis, thereby affecting septal cell wall synthesis and forming wider cells
459 with a lower surface-to-volume ratio³⁵. A sub-lethal dose (1.30 µg/mL) of NeACT significantly
460 inhibited *Sal1158c* efflux. The penetration of antimicrobials into the dense protective layer of
461 biofilms is crucial for their eradication. NeACT was highly effective in restricting biofilm growth
462 and inhibiting mature biofilms by accumulating and penetrating the biofilm layer.

463 The superior efficiency of NeACT against such resistance mechanisms of *Sal1158c* is
464 ascribed to the complementary mode of action of the antibiotic-adjuvant combinations. CF is
465 considered bactericidal as it binds to PBPs and interferes with cell wall enzymes, leading to cell
466 lysis and death. Although CPZ and TA are not known to inhibit bacterial growth at low dosages,
467 they contribute significantly to anti-efflux and antibiofilm properties, as observed in this study. TA
468 is a strong electron donor that interferes with the hydrolysis of ATP, causing an increase in bacterial
469 membrane permeability and thus enabling the passage of NeACT through the cell wall¹⁸. The free
470 phenolic hydroxyl groups in TA affect bacterial enzymatic activity *via* covalent or non-covalent
471 linking¹⁸. Moreover, TA has been reported to disrupt peptidoglycan formation, iron chelation, and
472 fatty acid synthesis¹⁸. CPZ complements the effect of TA and CF by crippling the function of
473 specific drug-resistance transporters and multidrug MFS efflux pumps and exhibiting
474 conformational changes in efflux protein structures^{36,37}. CPZ has also been reported to interact with
475 several membrane-active proteins, including FtsA and FabI, and exhibit strong anti-biofilm action



476 19. Moreover, CPZ has been reported to disrupt the sensor-inducer protein of the *S. aureus* cell
477 membrane and suppress *bla* and *mec* gene expression, which play a predominant role in producing
478 resistance factors such as PBP2a and β -lactamase²⁰. Additionally, chitosan-loaded CPZ exhibited
479 antibiofilm activity.

480 One of the prominent virulence characteristics that enables *S. aureus* to persist in mammary
481 tissue is its ability to invade and reside as an intracellular pathogen⁷. Therefore, we checked the
482 efficiency of NeACT in combating intracellular Sa1158c in Caco-2 cells. NeACT showed no
483 cytotoxicity and excellent remediation of intracellular Sa1158c. Earlier, our groups reported that
484 pristine CF and CPZ were marginally effective against intracellular pathogens^{7, 14}. As such, the
485 superior outcome observed in NeACT can be attributed to the combined impact of the drug
486 molecules and the favourable interaction and absorption of NeACT by the Caco-2 cells. To ensure
487 efficient cell interaction and intracellular transmission of a nanoparticulate system, a positive zeta
488 potential, such as that observed in NeACT, is crucial³⁸. Previous studies have shown that the
489 endocytic uptake of CH Np is significantly influenced by clathrin-mediated translocation³⁹. CD Np
490 undergoes macropinocytosis as the primary uptake mechanism in Caco-2 cells⁴⁰. It's likely that
491 NeACT utilizes a sequential release mechanism for its payloads. According to Zaki *et al.*, delivering
492 a high initial dose of antimicrobials inside cells, followed by a sustained antibiotic release, could be
493 an effective approach for treating intracellular infections. This method reduces relapses and ensures
494 efficient treatment⁴¹.

495 Clinical trials conducted in animals have revealed that nearly 30% of drug candidates
496 identified from preclinical screening fail due to toxic effects, while 60% do not deliver the desired
497 results⁴². This underscores the significance of exploring the efficacy of NeACT in treating BM
498 using *in vivo* models. Intraductal CD-1 lactating mice have been shown to accurately replicate *S.*



499 aureus-induced bovine mastitis, thereby serving as a valuable adjunct for *in vivo* research^{27, 43}.
500 NeACT demonstrated excellent remediation of Sa1158c infection by $\sim 5.13 \log_{10}$ and $\sim 4.46 \log_{10}$ in
501 the CD-1 mice mammary gland at a dosage of 78 and 39 $\mu\text{g/gland}$, respectively. Based on the
502 loading capacity of NeACT, the amounts of CF, CPZ, and TA contained in 39 $\mu\text{g/gland}$ of NeACT
503 were 12.53, 7.32, and 6.57 $\mu\text{g/gland}$, respectively. Histopathological examination suggested that the
504 exposure to NeACT neither induces inflammation nor impacts cell and tissue morphology. An
505 excessive amount of cell infiltration, along with classical immune cell activation, was observed in
506 infected mouse mammary glands, which led to tissue damage. Meanwhile, a minimal inflammatory
507 cell infiltration, as observed in NeACT-treated and infected mammary glands, is a crucial element
508 in the healing process. While the antibacterial effect of NeACT could be explained by the combined
509 action of CF and effector molecules, the components of NeACT could also influence the tissue
510 response to infection. Several studies have demonstrated the potential anti-inflammatory and
511 wound-healing properties of TA^{44, 45}. The exact mechanism through which TA exerts these effects
512 is not yet fully understood. However, scientific reports suggest that TA may stimulate healing by
513 modulating growth factors and activating the extracellular signal-regulated kinase 1/2 (ERK1/2)
514 pathway⁴⁴. Previous research has demonstrated that CH exerts anti-inflammatory effects by
515 modulating macrophage polarization from the pro-inflammatory M1 to the anti-inflammatory M2
516 state⁴⁶. In addition, it promotes an immune response that leads to the secretion of anti-inflammatory
517 mediators, such as the interleukin-1 receptor antagonist (IL-1ra) and interleukin-10 (IL-10)⁴⁶.
518 Previously, the CD was found to effectively decrease the concentration of various pro-inflammatory
519 cytokines, including interleukin-1 alpha (IL-1 α), tumor necrosis factor (TNF), and interleukin-6 (IL-
520 6)⁴⁷. All in all, our studies suggest that the design and choice of drug components are suitable for
521 ameliorating intramammary infection. The nanometric dimensions and surface chemistry are
522 thought to facilitate the penetration of NeACT into the tissue matrix (and bacterial biofilm, if



523 present), and the release of effective concentrations of antibiotics and effector molecules in the
524 vicinity of bacterial cells to eliminate the infection.

525

526 **5. Conclusion**

527 BM caused by microbial infections is one of the costliest diseases in the dairy industry
528 worldwide. The failure of conventional treatment and management strategies demands alternative
529 approaches. Nano-enabled Antibacterial Combination Therapy (NeACT) that harnesses the
530 potential of nano-delivery platforms for antibiotic/adjuvant combination of synergistic functions
531 holds promise in effective BM treatment. In this study, a NeACT was developed, consisting of CF-
532 loaded CH Np conjugated with CPZ and TA-loaded CD Np. NeACT demonstrated exceptional
533 stability, biocompatibility, slow-release behavior of payloads for efficient delivery, and successfully
534 remediated intracellular and intramammary infections of multi-drug-resistant MRSA. Future
535 clinical studies are needed to assess the efficacy, safety, and tolerability of NeACT in treating
536 mastitis in cattle. The fate of NeACT after achieving its therapeutic goals in the bovine mammary
537 gland requires extensive study. This includes evaluating the NeACT degradation, metabolism, and
538 impact on the host and the environment. As evidenced by our study, the slow-release behaviour of
539 payloads from nanocarriers can prolong their persistence in mammary tissue, thereby increasing the
540 risk of NeACT residues in milk, which in turn interferes with dairy processing and poses human
541 health concerns. Therefore, rigorous studies on the withdrawal period of NeACT are mandatory to
542 ensure milk safety, regulatory compliance, and consumer protection.

543

544



545 **Funding and Acknowledgements**

546 The authors acknowledge funding CRC/George/X-coded/248475 and CFI 254248 for supporting
547 this research work. This work was also supported by a team grant (no. 328798) from the Fonds de
548 Recherche du Québec – Nature et Technologie (FRQ-NT) to SG and FM, and we acknowledge
549 support from Op+lait, Regroupement stratégique FRQ-NT, pour un lait de qualité optimale
550 (Université de Montréal, St-Hyacinthe, QC, Canada). The authors thank Dr. Jennifer Ronholm,
551 McGill University, for providing the *Staphylococcus aureus* 1158c (Isolate ID: 10812464) and Sa30
552 (Isolate ID: 21000024) isolates. The authors thank the Facility for Electron Microscopy Research
553 (FEMR) and the Multiscale Imaging Facility, McGill University. The authors thank the Histology
554 and electron microscopy platform of Université de Sherbrooke. SM acknowledges student aid from
555 the McGill Graduate Excellence Award, and GM received an Alexandre-Graham-Bell doctoral
556 research studentship from the Natural Sciences and Engineering Research Council of Canada and a
557 studentship from FRQ-NT during this study.

558

559 **CRediT authorship contribution statement**

560 **Satwik Majumder:** Nanomaterial synthesis and characterization, *In-vitro* studies, Data curation,
561 Formal analysis, Investigation, Methodology, Validation, Visualization, Writing – original draft &
562 editing. **Guillaume Millette:** *In-vivo* study, Histology, Data curation, Formal analysis,
563 Methodology, Validation, Visualization. **Trisha Sackey:** *In-vitro* studies, Formal Analysis,
564 Methodology, Validation. **Francois Malouin:** Funding acquisition, Methodology, Resources,
565 Supervision, Validation. **Saji George:** Conceptualization, Funding acquisition, Investigation,
566 Project administration, Methodology, Resources, Supervision, Validation, Review & editing
567 manuscript.

568



569 **Declaration of Competing Interest**

570 The authors (Satwik Majumder, Guillaume Millette, Trisha Sackey, Francois Malouin, and Saji
571 George) declare that they have no known competing financial interests or personal relationships that
572 could have appeared to influence the work reported in this paper.

573

574 **Data availability**

575 The data supporting the findings of this study are provided in the paper and SI.

576



577 **References**

- 578 1. S. Majumder, P. D. Eckersall and S. George, *ACS Agricultural Science & Technology*, 2023,
579 **3**, 562-582.
- 580 2. W. N. Cheng and S. G. Han, *Asian-Australas J Anim Sci*, 2020, **33**, 1699-1713.
- 581 3. O. Kerro Dego, in *Animal Reproduction in Veterinary Medicine*, eds. F. Aral, R. Payan-
582 Carreira and M. Quaresma, IntechOpen, Rijeka, 2020, p. 93484.
- 583 4. G. Normanno, G. La Salandra, A. Dambrosio, N. Quaglia, M. Corrente, A. Parisi, G.
584 Santagada, A. Firinu, E. Crisetti and G. Celano, *International journal of food microbiology*,
585 2007, **115**, 290-296.
- 586 5. J.-H. Fairbrother, S. Dufour, J. M. Fairbrother, D. Francoz, É. Nadeau and S. Messier,
587 *Veterinary Microbiology*, 2015, **176**, 126-133.
- 588 6. S. Majumder, D. Jung, J. Ronholm and S. George, *BMC Microbiology*, 2021, **21**, 222.
- 589 7. S. Majumder, T. Sackey, C. Viau, S. Park, J. Xia, J. Ronholm and S. George, *BMC*
590 *Microbiology*, 2023, **23**, 43.
- 591 8. O. Kerro Dego and J. Vidlund, *Frontiers in Veterinary Science*, 2024, **11**, 1356259.
- 592 9. H. Barkema, Y. Schukken and R. Zadoks, *Journal of dairy science*, 2006, **89**, 1877-1895.
- 593 10. A. J. Bradley, J. E. Breen, B. Payne, V. White and M. J. Green, *Journal of Dairy Science*, 2015,
594 **98**, 1706-1720.
- 595 11. J. R. Middleton, J. Ma, C. L. Rinehart, V. N. Taylor, C. D. Luby and B. J. Steevens, *Journal of*
596 *Dairy Research*, 2006, **73**, 10-19.
- 597 12. S. Majumder, C. Viau, A. Brar, J. Xia and S. George, *Applied Clay Science*, 2022, **228**,
598 106569.
- 599 13. S. Majumder, J. Zhou and S. George, *LWT*, 2024, **210**, 116842.
- 600 14. A. Brar, S. Majumder, M. Z. Navarro, M.-O. Benoit-Biancamano, J. Ronholm and S. George,
601 *Nanomaterials*, 2022, **12**, 2179.
- 602 15. S. Majumder and S. George, in *Ayurvedic Herbal Preparations in Neurological Disorders*,
603 eds. M. Muralidhara and P. S. Rajini, Academic Press, 2023, pp. 611-633.
- 604 16. G. Truchetti, E. Bouchard, L. Descôteaux, D. Scholl and J. P. Roy, *Canadian Journal of*
605 *Veterinary Research*, 2014, **78**, 31-37.
- 606 17. J. P. Roy, L. DesCôteaux, D. DuTremblay, F. Beaudry and J. Elsener, *Canadian Veterinary*
607 *Journal*, 2009, **50**, 1257-1262.
- 608 18. X. Villanueva, L. Zhen, J. N. Ares, T. Vackier, H. Lange, C. Crestini and H. P. Steenackers,
609 *Frontiers in Microbiology*, 2023, **13**, 987164.
- 610 19. S. Nistorescu, G. Gradisteanu Pircalabioru, A.-M. Udrea, Á. Simon, M. L. Pascu and M.-C.
611 Chifiriuc, *Coatings*, 2020, **10**, 1230.
- 612 20. R. Kong, O.-H. Kang, Y.-S. Seo, S.-H. Mun, T. Zhou, D.-W. Shin and D.-Y. Kwon, *Asian Pacific*
613 *Journal of Tropical Medicine*, 2016, **9**, 542-546.
- 614 21. P. Yadav, A. B. Yadav, P. Gaur, V. Mishra, Z. I. Huma, N. Sharma and Y. O. Son,
615 *Biomedicines*, 2022, **10**, 3282.
- 616 22. G. Tiwari, R. Tiwari and A. K. Rai, *Journal of Pharmacy and Bioallied Sciences*, 2010, **2**, 72-
617 79.
- 618 23. C. Stein, O. Makarewicz, J. A. Bohnert, Y. Pfeifer, M. Kesselmeier, S. Hagel and M. W. Pletz,
619 *PLOS One*, 2015, **10**, e0126479.
- 620 24. N. M. Soliman, F. Shakeel, N. Haq, F. K. Alanazi, S. Alshehri, M. Bayomi, A. S. M. Alenazi and
621 I. A. Alsarra, *Molecules*, 2022, **27**, 4468.
- 622 25. L. Shao, S. Majumder, Z. Liu, K. Xu, R. Dai and S. George, *Journal of Photochemistry and*
623 *Photobiology B: Biology*, 2022, **231**, 112450.

624 26. J. M. Radziwill-Bienkowska, P. Talbot, J. B. J. Kamphuis, V. Robert, C. Cartier, I. Fourquaux,
625 E. Lentzen, J.-N. Audinot, F. Jamme, M. Réfrégiers, J. K. Bardowski, P. Langella, M.
626 Kowalczyk, E. Houdeau, M. Thomas and M. Mercier-Bonin, *Frontiers in Microbiology*, 2018,
627 **9**, 794.

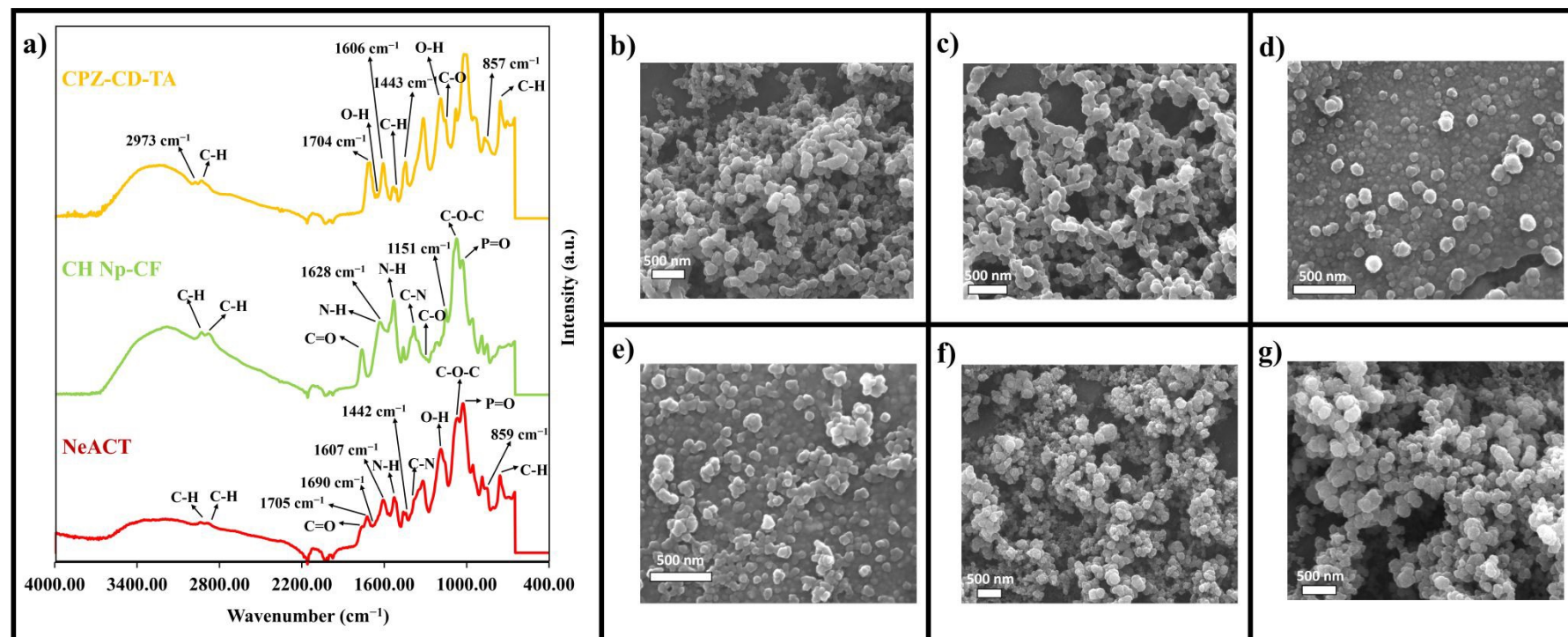
628 27. E. Brouillette, G. Grondin, C. Lefebvre, B. G. Talbot and F. Malouin, *Veterinary Microbiology*,
629 2004, **101**, 253-262.

630 28. E. Brouillette, G. Grondin, B. G. Talbot and F. Malouin, *Veterinary Immunology and*
631 *Immunopathology*, 2005, **104**, 163-169.

632 29. S. Sana, S. Datta, D. Biswas and D. Sengupta, *Biochimica et Biophysica Acta (BBA) -*
633 *Biomembranes*, 2018, **1860**, 579-585.

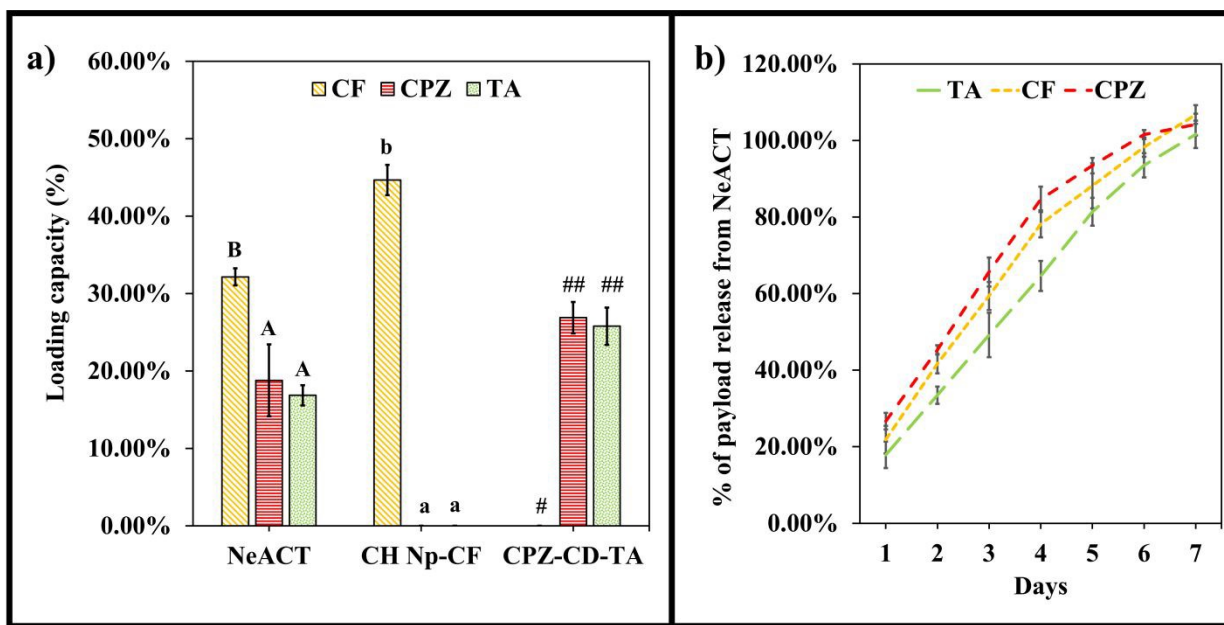
634



635 **Figures**

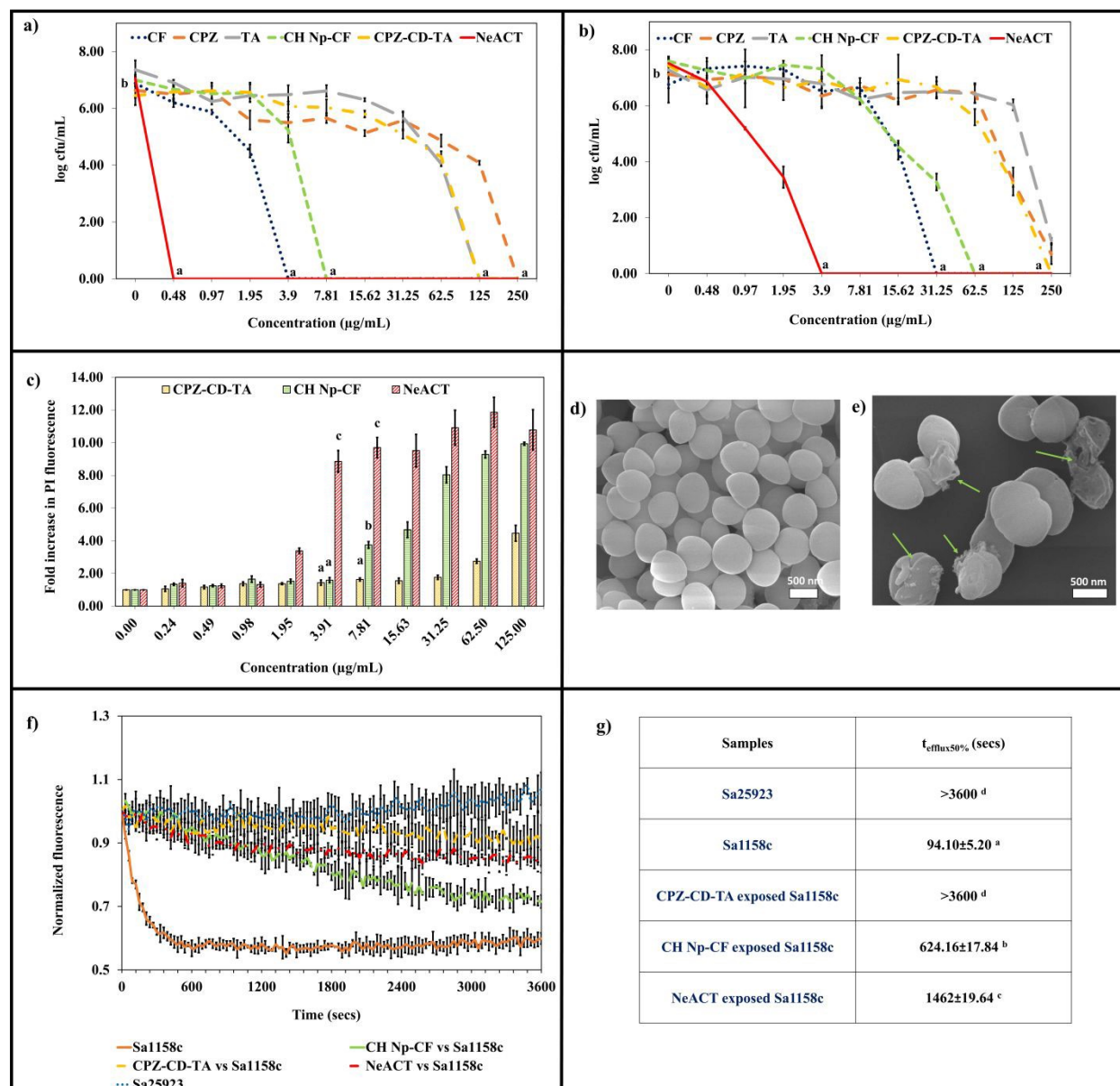
636

637 **Figure 1. Physicochemical characterization of the particles.** (a) FT-IR analysis of the particles analyzed at a wavelength range of 600–
638 4000 cm^{-1} with a resolution of 4 cm^{-1} . Scanning electron microscopy (SEM) images of (b) CD-NP, (c) CPZD-CD-TA, (d) CH Np, (e) CH CF-
639 Np, (f–g) NeACT. The particles were dropped onto aluminium mounts, dried, and coated with platinum. The images were acquired using an
640 SEM.



641

642 **Figure 2. Loading capacity of particles and release profile of the payloads. (a)** The loading
643 capacity of the particles for CF, CPZ, and TA. The particles of 1 mg/mL were centrifuged and
644 filtered. An HPLC system was used to assess the availability of CPZ, TA, and CF in the particles.
645 **(b)** The release profile of CF, CPZ, and TA from NeACT. The release of CF, CPZ, and TA was
646 checked every 24 h for seven days. NeACT of 1 mg/mL was centrifuged gently, and the supernatant
647 was collected. HPLC was used to assess the percentage of payload release. Average values plotted
648 in the graph with different alphabets and symbols indicate a significant difference ($p < 0.05$).



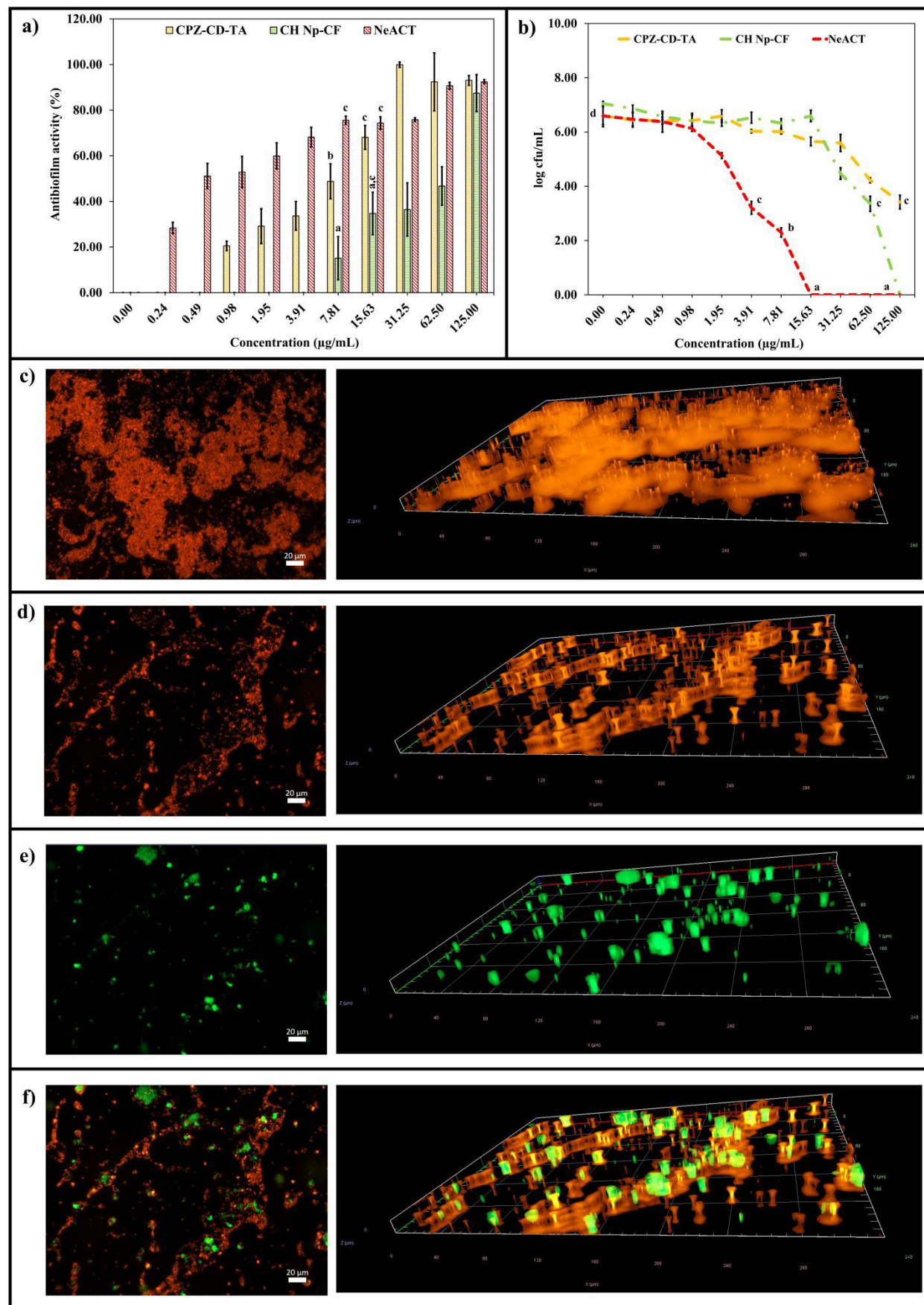
649

650 **Figure 3. Antibacterial efficiency and mechanism of action of particles against *S. aureus*. (a-**
 651 **b)** Antibacterial efficacy of NeACT and control groups against (a) Sa25923 and (b) Sa1158c. In a
 652 96-well plate, the incremental concentration of the samples was subjected to MHB media
 653 containing bacteria maintained at 0.5 McFarland standard. The plate was incubated for 18 h, and
 654 the CFU was enumerated using the drop plate culturing method. (c) Sa1158c membrane integrity
 655 upon particle exposure. After 6 h of incubation, PI dye was added to the wells. The fluorescence
 656 intensity was measured at an excitation/emission wavelength of 555/645 nm using a plate reader.



657 Average values plotted in the graph with different alphabets indicate a significant difference
658 ($p < 0.05$). **(d-e)** SEM image of **(d)** untreated Sa1158c cells and **(e)** NeACT-treated Sa1158c cells.
659 Bacterial cells were exposed to sub-lethal concentrations of NeACT for 6 h. The cells were
660 harvested, washed, and fixed with 2.5% glutaraldehyde. Critical point drying was performed, and
661 the cells were coated with platinum and examined under SEM. Green arrows indicate
662 compromised membrane integrity. **(f-g)** Efflux pump inhibition property of the particles. Sa1158c
663 culture was subjected to a sub-lethal concentration of the particles followed by a sub-lethal dosage
664 of EtBr. The cells were harvested, washed, and transferred to a 96-well plate. Glucose was added,
665 and EtBr efflux was monitored at an excitation/emission wavelength of 530/590 nm using a plate
666 reader. A single exponential decay equation was used to determine the time-dependent efflux of
667 EtBr. The time taken by the cells to extrude 50% of the EtBr was denoted as $t_{\text{efflux}50\%}$. Average
668 values plotted in the table and graph with different alphabets indicate a significant difference
669 ($p < 0.05$).

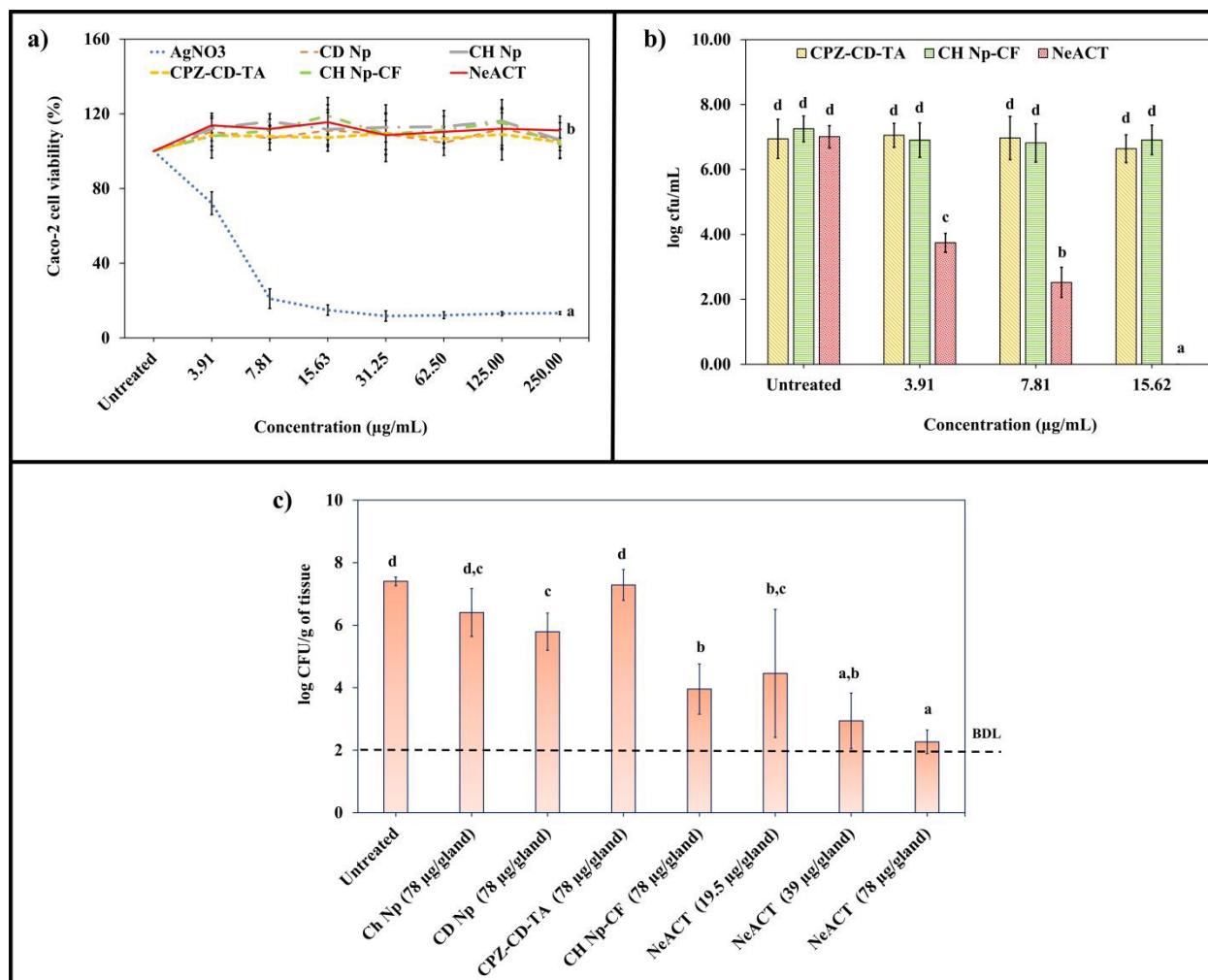




671 **Figure 4. Mechanism of action of the particles against *S. aureus* biofilms. (a)** Antibiofilm
672 activity of the particles. Incremental concentrations of the particles were suspended in TSB media
673 containing Sa1158c culture. After 48 h of incubation, the media was removed, 99% methanol was
674 added, wells were washed gently, and resuspended with CV solution. The plates were incubated for
675 2 h, washed, and acetic acid (33%) was added. The biofilm biomass was quantified by measuring
676 the absorbance at 570 nm. **(b)** Inhibition of matured biofilms by the particles. Matured biofilms
677 formed after 24 h of incubation were exposed to incremental concentration of the particle in a 96-
678 well plate. The plate was incubated for 24 h. The biofilms were collected, and the CFU was
679 enumerated using the drop plate culturing method. Average values plotted in the graph with different
680 alphabets indicate a significant difference ($p < 0.05$). **(c-f)** Epifluorescence and Z-stack images of
681 **(c)** untreated RFP-tagged Sa30 biofilms, **(d)** treated RFP-tagged Sa30 biofilms, **(e)** FITC-NeACT
682 signal in Sa30 biofilms, and **(f)** overlapped signals of FITC-NeACT penetrating RFP tagged Sa30
683 biofilms. A sub-lethal dosage of FITC-NeACT was exposed to matured biofilms of RFP-tagged
684 SA30. Cell Discoverer 7 was used to capture epi-fluorescence images of the biofilms (coding red at
685 583 nm) and FITC NeACT (coding green at 519 nm). Z-stack images of different layers were
686 constructed.

687

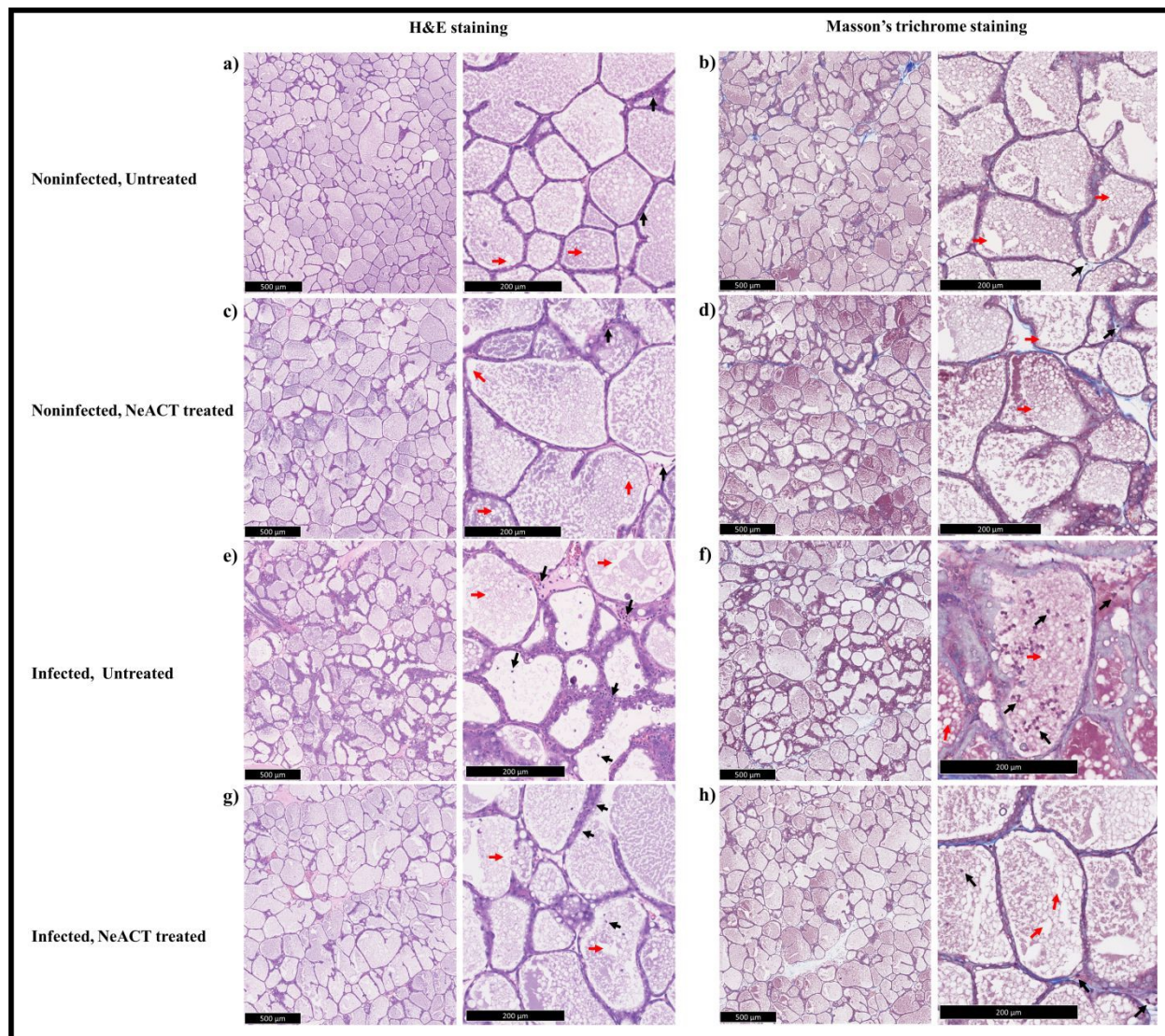




688 **Figure 5. Cytotoxicological assessment and intracellular infection remediation study in Caco-2**
689 **cells and *in vivo* efficiency of the particles in infected CD-1 lactating mice model. (a)**
690 **Cytotoxicity of the particles in Caco-2 cells.** Confluent cells (2×10^4 cells/well) were exposed to an
691 incremental concentration of the particles in DMEM media in a 96-well plate. After 24 h of
692 incubation, resazurin was added to the wells, and the plate was incubated for 4 h further.
693 Fluorescence intensity was measured at 530/590 (excitation/emission). **(b)** Intracellular Sa1158c
694 remediation efficiency of the particles. Confluent Caco-2 cells were exposed to Sa1158c culture and
695 incubated in a 96-well plate for an hour. The cells were washed, subjected to gentamicin, and
696 incubated for 30 min. The extracellular gentamicin was washed, and the plate was incubated with
697

698 DMEM for 4 h. Incremental concentrations of the particles were added to the wells and incubated
699 for 24 h. Further, the cells were washed and lysed using Triton X. Drop culture method was used
700 for CFU enumeration of viable intracellular Sa1158c. Average values plotted in the graph with
701 different alphabets indicate a significant difference ($p < 0.05$). **(c)** Sa1158c infection remediation
702 efficiency of the particles from CD-1 lactating mice mammary glands. Sa1158c of 100-125 CFUs
703 were injected into the lactiferous duct of CD-1 lactating mice. Certain concentrations of the particles
704 were directly injected into the mammary glands previously infected. After 14 h of incubation, mice
705 were humanely euthanized, and mammary glands were harvested and homogenized. CFU counts
706 were obtained from mammary gland homogenates on TSA plates. The detection limit was
707 approximately 200 CFU/g of mammary glands. Average values plotted in the graph with different
708 alphabets indicate a significant difference ($p < 0.05$).





709
 710 **Figure 6. Histopathological analysis of CD-1 mice mammary tissue. (a)** H&E staining and **(b)**
 711 Masson's trichome staining of noninfected and untreated mammary tissue. **(c)** H&E staining and
 712 **(d)** Masson's trichome staining of noninfected but NeACT-treated mammary tissue. **(e)** H&E
 713 staining and **(f)** Masson's trichome staining of infected but untreated mammary tissue. **(g)** H&E
 714 staining and **(h)** Masson's trichome staining of infected and NeACT-treated mammary tissue. The
 715 mammary glands were fixed in 4% PFA, dehydrated, and embedded in paraffin. Tissue preparation,
 716 embedding, and coloration were performed by the Electron Microscopy and histology platform at



717 the Université de Sherbrooke. The black and red arrows denote the PMN infiltration and adipocytes,
718 respectively.



719 **Table**

720

Samples	Hydrodynamic size (nm)	Zeta potential (mV)
CD Np	137.41±5.91	-11.37±1.37
CH Np	269.56±3.43	+29.89±0.62
CH Np-CF	309.52±5.11	+30.68±1.21
CPZ-CD-TA	132.77±4.84	-9.51±1.56
NeACT	539.58±12.36	+21.69±2.43

721

722 **Table 1. The hydrodynamic size and zeta potential of the particles.**

Data availability

The data supporting the findings of this study are provided in the paper and SI.

